14th International Symposium on Turbulence and Shear Flow Phenomena (TSFP14)
Heidelberg, Germany, July 28–31, 2026

ECCENTRICITY EFFECTS ON UPWARD GAS-LIQUID FLOW REGIMES IN VERTICAL ANNULAR CHANNELS

Egemen Bilgin
Department of Mechanical Engineering
University of Ottawa
Ottawa, ON K1N 6N5, Canada
ebilg081@uottawa.ca

Stavros Tavoularis
Department of Mechanical Engineering
University of Ottawa
Ottawa, ON K1N 6N5, Canada
stavros.tavoularis@uottawa.ca

ABSTRACT

Experimental and computational studies of air-water mixtures flowing upwards in concentric and eccentric vertical annular channels were performed. Videos taken from two directions perpendicular to each other were analysed visually at low speed. Four regimes were identified, namely, bubbly, cap-bubbly, slug and churn flows. A flow regime map was constructed for the full range of eccentricity e. It was observed that the boundaries between regimes in the map were shifted with changes in eccentricity in the range $0.3-0.7$. Oscillatory cross flows were identified both in the video recordings of bubbly, cap-bubbly and slug flow regimes for $e = 0.5$ and 0.7 and in the numerical simulations at corresponding conditions. These cross flows are attributed to gap vortex streets and are the main source of eccentricity effects on regime transition.

INTRODUCTION

Multiphase flows can be classified into five types: gas-liquid, gas-solid, liquid-solid, immiscible liquid-liquid, and gas-liquid-solid ones. Because of the compressibility of gases and the deformability of liquids, gas-liquid flows are considered to be the most complex two-phase flow type. Gas-liquid flows are commonly encountered in thermal power generation plants, petroleum extraction systems and chemical industries. Among the engineering systems and processes in which the prediction of gas-liquid flow characteristics is essential, one may mention nuclear reactor cores supplied with emergency coolant, steam boilers and heat exchangers, gas absorption units, oil and gas wells, fuel pipelines, activated sludge processes and polymer devolatilisation. The characteristics of gas-liquid flows depend on the geometry of the vessel, the fluid properties and the flow orientation with respect to the gravitational direction. The main geometrical parameters for flows in annular channels are the ratio $\gamma = D_{in}/D_{out}$ of the inner D_{in} and outer D_{out} diameters of the annulus and the eccentricity $e = 2\delta/(D_{out} - D_{in})$, where δ is the distance between the axes of the inner and outer cylinders. Due to imperfections in manufacturing and wear, annular channels in engineering systems unavoidably have some eccentricity. The dynamic conditions of a gas-liquid flow in an annular channel are characterised by the inverse viscosity number $N_f = [\rho_l(\rho_l - \rho_g)gD_h^3]^{1/2}/\mu_l$, the Eötvös number $Eo = (\rho_l - \rho_g)gD_h^2/\sigma$ and the Morton number $Mo = (\rho_l - \rho_g)g\mu_l^4/(\rho_l^2\sigma^3)$, where ρ_l, ρ_g are, respectively, the densities of the liquid and the gas, $D_h = D_{out} - D_{in}$ is the hydraulic diameter, μ_l is the viscosity of the liquid and σ is the surface tension.

A main characteristic of gas-liquid flows is the flow regime, which describes the pattern of the distribution of two phases Hetsroni (1982); Brennen (2005). Although the terminology used by different authors may vary somewhat, it is recognised that, in upward vertical flows in pipes and channels, there are four main flow regimes: bubbly flow, slug flow, churn flow and annular flow. Additional flow regimes described in the literature are cap-bubbly flow, dispersed bubble flow, mist flow, wispy annular flow and dispersed droplet flow. The conditions for the occurrence of flow regimes are summarised in maps, usually presented in terms of the gas and liquid superficial velocities, respectively, j_g and j_l. Transition from one regime to another typically occurs by coalescence or breakdown of bubbles, as conditions change. Gas-liquid regime maps for circular and rectangular channels have been presented by many authors (Oshinowo & Charles, 1974; Taitel *et al.*, 1980; Sadatomi *et al.*, 1982; Mishima & Ishii, 1984; Barnea, 1987; Hibiki & Mishima, 2001). Upward gas-liquid flow regime maps for concentric vertical annular channels have also been reported (Kelessidis & Dukler, 1989; Caetano *et al.*, 1992*a*; Das *et al.*, 1999; Hibiki *et al.*, 2003; Sun *et al.*, 2004; Ozar *et al.*, 2008; Julia *et al.*, 2009; Julia & Hibiki, 2011; Julia *et al.*, 2011; Guo *et al.*, 2018; Yin *et al.*, 2025), but such maps for eccentric vertical annular channels are only available for $e = 0.5$ (Kelessidis & Dukler, 1989, 1990) and $e = 1$ (Caetano *et al.*, 1992*a*,*b*; De Sousa *et al.*, 2014).

Previous literature (Tavoularis, 2011; Choueiri & Tavoularis, 2014, 2015; Lamarche-Gagnon & Tavoularis, 2021) has shown that single-phase flows in eccentric annular channels, rod bundles and other channels with axial gaps are subject to the mechanism of gap instability, which, under certain conditions, may generate a street of quasi-periodic, staggered, counter-rotating vortex pairs. Gap vortices transport fluid across the gap and generate strong cross flows in the entire cross section. The possible presence of gap vortex streets in gas-liquid flows in eccentric annular channels and its effects on the flow pattern and other characteristics have never been investigated in the literature. The presence of gas-filled bubbles disrupts the continuity of the liquid phase, thus complicating the structure of any existing gap vortices. Nevertheless, because the vortex street has a relatively long wavelength, it seems unlikely that cross flows would be annihilated by relatively small bubbles, at least in the bubbly and cap-bubbly regimes and possibly in the slug flow regime. Investigations of these phenomena seem worthwhile, first because they would illuminate some interesting and complex flow phenomena and second for their potentially important practical consequences.

METHODOLOGY
Experimental methodology

A sketch of the flow facility is shown in Fig. 1. The test section has the same annular channel configuration as the horizontal annular channel described by Lamarche-Gagnon & Tavoularis (2021). It consists of an outer glass tube with a diameter $D_{out} = 37$ mm $\pm$ 1% and and an inner glass tube with a diameter $D_{in} = 18$ mm $\pm$ 1%. These give a diameter ratio $\gamma = 0.49$, a hydraulic diameter $D_h = 19$ mm, and an ideal area-equivalent circular tube diameter $D_{ideal} = \sqrt{D_{out}^2 - D_{in}^2} = 32.3$ mm. The test section length is $L \approx 3$ m $\approx 158D_h \approx 93D_{ideal}$. A cross-sectional view of the test section is shown in Fig. 2. Flow entered the test section bottom through a bell-shaped "trumpet" with an ellipsoidal profile and an area ratio of 4.2. At its bottom, the inner tube was terminated and sealed by an inlet coupling, which also had an ellipsoidal shape to facilitate a smooth inlet into the annular channel. A threaded rod with side spacers was placed inside the entire length of the inner tube. This rod was fastened at its upper end on a horizontal traversing mechanism, which was immersed in the upper tank, and at its bottom end onto the inlet coupling of the inner tube. The threaded rod allowed the inner tube to be suspended from the top and free at its bottom. The eccentricity of the inner tube was adjusted at three different elevations: at the top, via the traversing mechanism, powered by a servomotor; in the middle, via two stainless steel precision pins with a diameter of 1 mm; and, at the bottom, with the use of stainless steel wires with a 0.3 mm diameter, which were mounted on opposite sides of the inner tube, penetrated through the trumpet and were kept taut by guitar tuning pegs. For all tests, the upper tank was left open to the atmosphere. The upper and bottom tanks were connected in a closed loop and water was circulated by a magnetic-drive pump (Iwaki, Model MD-70RLT). The pump motor speed was kept fixed during the tests and the water flow rate through the test section was controlled by a bypass valve, which diverted part of the flow to a separation tank where trapped air in the return flow was vented. The water flow rate was measured with a calibrated ultrasonic flowmeter (OMEGA, Model FTD-31-T). Air was released through a solenoid valve in the bottom tank below the test section at a regulated pressure P_r and the air flow rate was measured with one of two rotameters having different operating ranges.

Two simultaneous, perpendicular to each other, views of the flow in a part of the test section that was enclosed in a viewing tank filled with water were recorded at a rate of 100 fps by two video cameras (pco.edge sCMOS and pco.edge 5.5 CLHS sCMOS, Excelitas PCO GmbH, Germany) to be referred to as

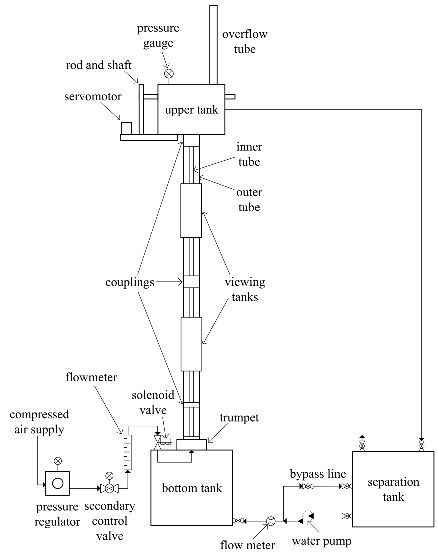

Figure 1. Sketch of the experimental setup.

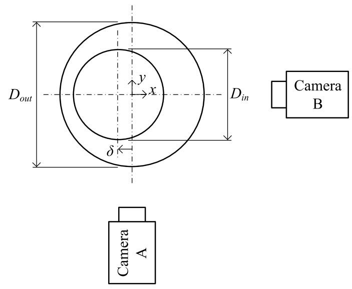

Figure 2. Sketch of the annular channel and the cameras.

Camera A and Camera B (see Fig. 2).

The uncertainty of eccentricity along the test section was about 0.05. The resolution of the pressure gauge, approximated as half of the scale increments on the gauge, was 1.7 kPa. The ultrasonic flowmeter measured the liquid flow rate within 1%. The resolution for the lower-range rotameter was 0.003 m^3/h and the resolution of the wider-range rotameter was 0.071 m^3/h.

Computational methodology

Computational studies of air-water flows in annular channels at conditions matching the experimental ones were conducted using the Volume of Fluid (VOF) method to resolve the gas-liquid interface and the Improved Delayed Detached Eddy Simulation (IDDES) with the SST (Menter) $k-\omega$ model to model turbulence in the liquid. All simulations were performed using the commercial finite volume CFD package Star-CCM+. Multiple cases were run simultaneously on local servers at the University of Ottawa and on servers available through the Digital Research Alliance of Canada. Each of these cases took approximately 4 months of CPU time in local computers (44 processors) and $1-2$ months in Alliance Canada computers ($128-256$ processors)

The computational domain is shown in Fig. 3. Its cross section was the same as the experimental one, but its height was $L_c = 20D_{out} = 0.74$ m, namely shorter than the experimental test section, in order to keep the computational time within tolerable levels. Previous studies (Kiran *et al.*, 2020; Liu *et al.*, 2024) have shown that such a length would be sufficient for the flow to reach an approximately fully developed state. The computational domain was discretised using an automated mesh generator, which interfaced polyhedral cells away from the wall with near-wall prismatic layers and enacted a surface remeshing, as shown in Fig. 3. Extensive mesh dependence studies were performed for the analysis of Taylor bubbles rising in a stagnant water column through the same test section (Bilgin, 2026). Based on these studies, we generated a mesh with 3.7 million cells for the present simulations; this mesh was deemed to provide sufficient accuracy and resolution for the present, largely qualitative, purposes. At the inlet of the annular channel, air was injected with a uniform velocity through a round orifice with an area of 8 mm^2, whereas water with also a uniform velocity was injected through the remainder of the inlet cross section. The side boundaries of the inner and outer tubes were set as walls, whereas the outlet at the top was left open to the atmospheric pressure. The initial condition was to fill the entire domain with water at the same uniform velocity as the water inlet. An adaptive time-step control was used with a targeted mean Courant number of 0.5 and a minimum time step of 10^{-5} s.

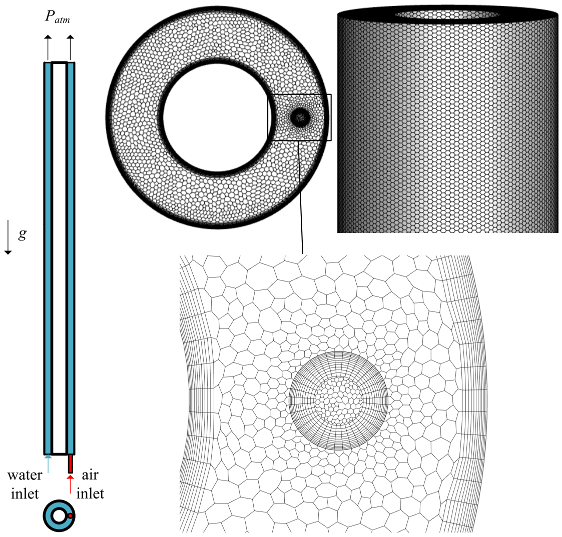

Figure 3. Computational domain and boundary conditions (left); cross-sectional and axial meshes (right).

RESULTS AND DISCUSSION

Experimental and computational conditions

Experiments were conducted for the full range of eccentricity ($e = 0, +0.3, +0.5, +0.7, +1$) and wide ranges of water and air flow rates, presented in the form of corresponding superficial velocities ($0.032 < j_l < 0.292$ m/s and $0.006 < j_g < 2.028$ m/s). The values of the main dimensionless parameters were $N_f = 8{,}300$, $Eo = 49$ and $Mo = 2.3 \times 10^{-11}$. Numerical simulations were run for three eccentricity values, namely, $e = 0.3, 0.5$ and 0.7, at approximately the maximum experimental liquid superficial velocity ($0.27 < j_l < 0.29$) and four gas superficial velocities ($j_g = 0.006, 0.074, 0.144$ and 2.028 m/s, adjusted to correspond to $H = 2.8$ m). Thus, a total of 12 simulations were performed, at conditions approximating experimental conditions at which all four flow regimes were observed. Performing additional simulations would exceed the time that was available for this work.

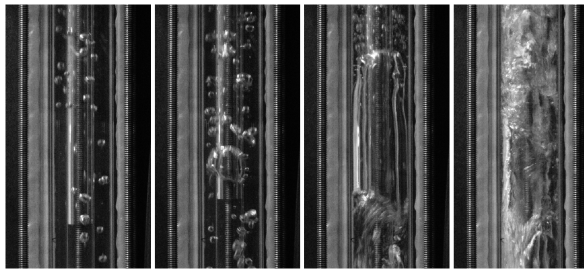

Figure 4. Representative images of flow patterns: bubbly flow, cap-bubbly flow, slug flow and churn flow (left to right).

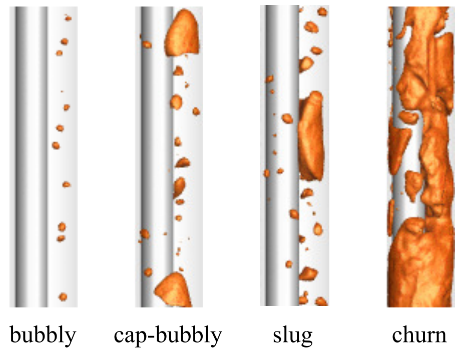

Figure 5. Isosurfaces of the volume fraction of air ($\alpha_g \geq 0.9$) on the $y - z$ plane for $e = 0.7$.

Observed flow regimes

The flow regime was identified by visual observation of the flow in real time and by inspecting videos of the flow through the upper viewing tank ($H = 2.8$ m), replayed at a lower speed when necessary. Four flow regimes were identified, namely, the bubbly, the cap-bubbly, the slug, and the churn regime, representative images of which are shown in Fig. 4. The bubbly flow contained only small, nearly spherical bubbles, which did not coalesce to create larger ones. The cap-bubbly flow contained short cap bubbles, which had a length that was less than D_h and a shape resembling the nose region of Taylor bubbles. As the gas flow rate was increased, cap bubbles grew into Taylor bubbles, the length of which increased with increasing flow rate. Further increase in gas flow rate made the Taylor bubbles coalesce with each other and create very long bubbles with lengths exceeding $30D_h$, while the liquid slugs between these bubbles became shorter and developed an increasingly frothy appearance. Once these long bubbles started to coalesce with each other, they became highly distorted, with liquid occasionally dropping through the gas. Under such conditions, the regime was identified as churn flow. It is noted that the transition from slug to churn flow was not as obvious as the transition from bubbly to cap bubbly flow and from cap bubbly to slug flow. This is in agreement with the observation of Cao *et al.* (2024).

All four regimes that were observed experimentally were also found by computations at comparable conditions; examples of these are shown in Fig. 5. It is noted, however, that, if the computational domain were longer, it is possible that, under certain conditions, additional transitions may have occurred. In any case, the CFD results are used primarily for supporting the experimental evidence for the occurrence of cross flows and not for characterising regime transitions.

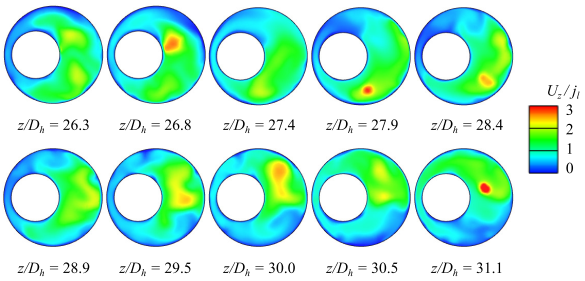

Figure 6. Simultaneous flood maps of the axial velocity on closely spaced $x-y$ planes in bubbly flow for $e = 0.7$.

Evidence for the presence of cross flows

Observation of video recordings of air-water flows replayed at low speed demonstrated that, at least for eccentricities in the range $0.5 \lesssim e \lesssim 0.7$, both dispersed and cap bubbles had roughly quasi-periodic cross motions of a type that is consistent with the actions of gap vortex streets. Circumferential motions were also observed in slug flow, but it was not clear whether these motions were due to gap vortices or an instability of the turbulent wakes of the liquid slugs. No reliable assertion can be made for circumferential motions in the churn flow regime due to the chaotic nature of such flows. On the other hand, numerical simulations for $e = 0.7$ revealed the presence of strong oscillatory cross flows in all four regimes. These observations were made by the inspection of instantaneous cross-sectional maps of the normalised axial velocity U_z/j_l, computed simultaneously at multiple axial locations of the eccentric annular channels. Near the inlet ($z/D_h \leq 10.5$), these maps did not differ from each other significantly as the fluid velocity was not far from being uniform. Around mid-channel and beyond ($z/D_h \geq 20$), however, significant differences between the axial speeds in the narrow and wide gap regions, as well as oscillatory circumferential motions, were observed. Representative axial velocity maps shown in Fig. 6 demonstrate that the high axial velocity region (denoted by green colour in the images) swung strongly circumferentially. The amplitude of cross motion became larger with an increase in eccentricity from 0.3 to 0.7. From these images, one may estimate very roughly the axial wavelength of the oscillations as $10D_h \approx 10D_{in}$. The present findings are in fair qualitative agreement with results by Choueiri & Tavoularis (2014) and many other authors and clearly prove the presence of gap vortex streets in eccentric channels.

Regime transitions

A flow regime map for all eccentricities is shown in Fig. 7. This map covers all four regimes that were discussed previously. For a fixed liquid flow rate within the entire range of values tested, the flow regime progressed from bubbly to churn flow as the gas flow rate was increased. In most of the map, the flow was in the same regime for all eccentricities, however, the boundaries between regimes shifted as eccentricity changed. In other words, eccentricity did not affect the type of regime away from transition regions, but, near transition regions, a change in eccentricity could trigger transition from one regime to another. The transition regions have been marked by shaded areas in Fig. 7, but, because the symbols for different eccentricities largely overlap, it is not possible to discern clearly the effect of eccentricity. Even so, the following general observation can be made: regardless of eccentricity, all transitions were shifted towards higher gas flow rates as the liquid flow rate was increased. Thus, the transition areas of

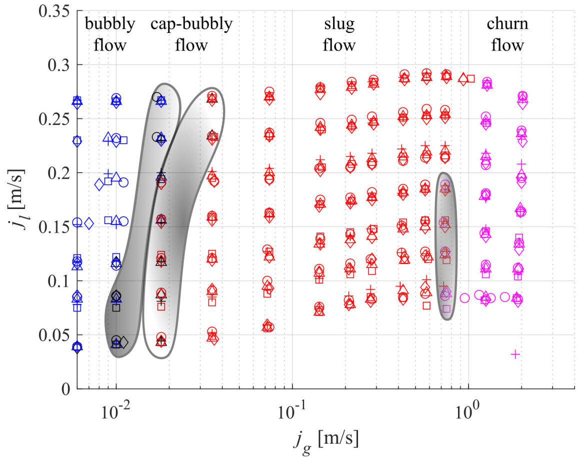

Figure 7. Regime map of air-water flows in annular channels with $e = 0$ (△), 0.3 (□), 0.5 (◇), 0.7 (◯), and 1 (+); symbols are blue for bubbly flow, black for cap-bubbly flow, red for slug flow, and magenta for churn flow.

the map were tilted clockwise; this tilt is obvious for the two transitions at lower j_g and may be inferred for the higher-j_g transition, where the data density is relatively low.

Experiments were performed for 13 specific values of j_g and a wide range of j_l. For nine values of j_g, the flow regime was the same for all eccentricities, but, each of four sets, those with $j_g = 0.010, 0.018, 0.035$ and 0.70 m/s and different eccentricities, had cases with different flow regimes. To illustrate this effect, we have drawn regime maps in axes of e and j_l for the previously mentioned four values of j_g. In general, these maps demonstrate that eccentricity affects measurably the conditions for transition from one regime to another and that this effect does not depend monotonically on e, but is strongest for intermediate values of e. For $j_g = 0.010$ m/s (Fig. 8), bubbly flow was observed for all j_l examined, when $e = 0$ and 1, but, for intermediate eccentricities, bubbly flow occurred when j_l exceeded a specific threshold, which depended on e, whereas cap-bubbly flow occurred when j_l dropped below this threshold. For $j_g = 0.018$ m/s (Fig. 9), two flow regimes, bubbly and cap-bubbly flows, were observed, when $e = 0$ and 1, but, for intermediate eccentricities, three regimes, bubbly, cap-bubbly and slug flows occurred. Representative images of flows in these three regimes are shown in Fig. 10. For $j_g = 0.035$ (Fig. 11), only a small part of the map ($e = 0, j_l \gtrsim 0.2$ m/s) was in cap-bubbly flow, whereas the rest of the map was in slug flow. Although this figure, viewed in isolation, cannot describe the general effect of eccentricity on regime transition, it does illustrate that such effect exists and shows a transition trend that is consistent with the trends that may be extracted from the general regime map (Fig. 7). For $j_g = 0.70$, the void fraction was relatively high for all examined j_l and only two flow regimes were observed: slug flow occurred when j_j exceeded a threshold that depended on e and churn flow occurred when j_l dropped below this threshold. Although for $e = 1$ the map does not extend to sufficiently low values of j_l for slug-to-churn-flow transition to be observable, one may infer that such transition would have occurred if j_l were dropped below the lowest value in the tests. This figure shows that, for $e = 0.7$, transition occurred at a value of j_l that was more than twice the transition threshold for the concentric channel and for channels with low eccentricities.

We now proceed to explain how gap vortices could af-

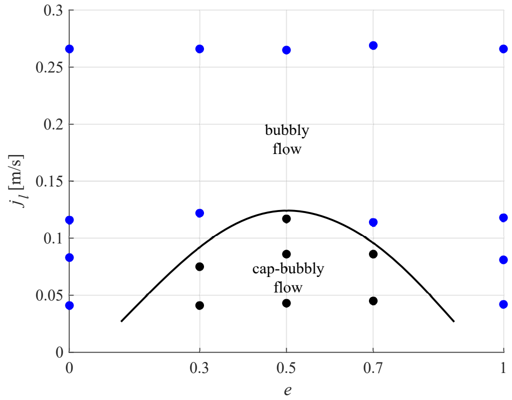

Figure 8. Flow regime map for $j_g = 0.010$ m/s; symbols are blue for bubbly flow and black for cap-bubbly flow; the line marks the approximate boundary between regimes.

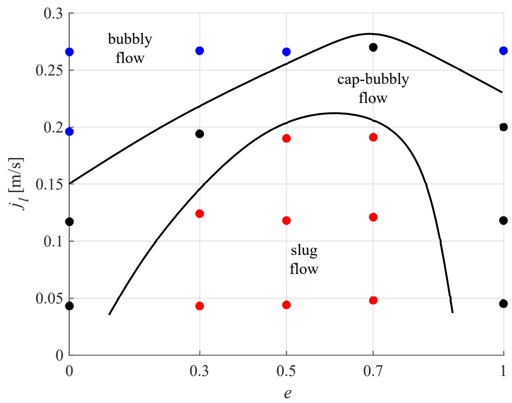

Figure 9. Flow regime map for $j_g = 0.018$ m/s; symbols are blue for bubbly flow, black for cap-bubbly flow and red for slug flow.

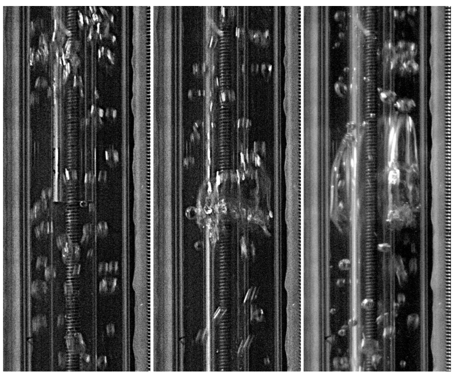

Figure 10. Representative images of flow patterns near flow transition boundaries for $e = 0.3$ and $j_g = 0.018$ m/s; left: bubbly flow ($j_l = 0.267$ m/s); centre: cap-bubbly flow ($j_l = 0.194$ m/s); and right: slug flow ($j_l = 0.124$ m/s).

fect the flow regime boundaries. Because air has much lower inertia than water, gas bubbles would tend to oscillate with larger amplitudes, thus larger velocities, than the adjacent liquid. Therefore, the magnitude of the velocity of bubbles would tend to increase significantly above their axial velocity component, which is accounted for by the superficial velocity of

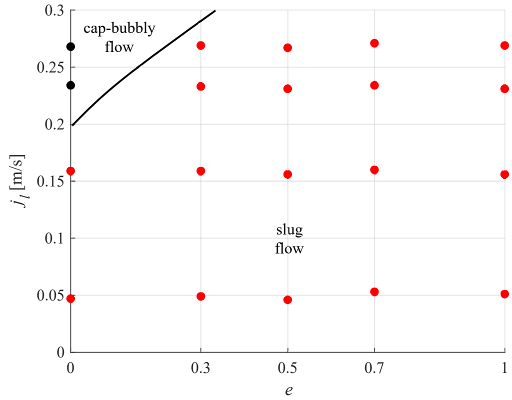

Figure 11. Flow regime map for $j_g = 0.035$ m/s; symbols are black for cap-bubbly flow and red for slug flow.

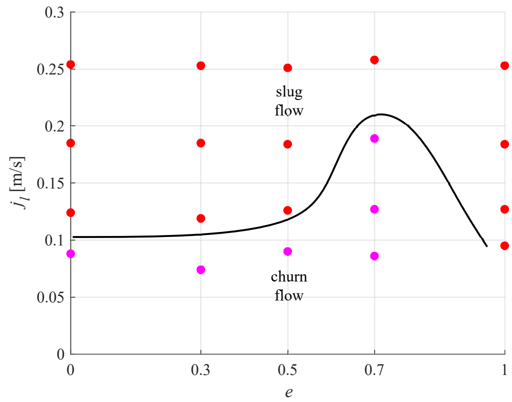

Figure 12. Flow regime map for $j_g = 0.70$ m/s; symbols are red for slug flow and magenta for churn flow.

air. Bubbles embedded in different parts of a liquid vortex would have different velocity magnitudes and directions and so the probability of bubble collisions and coalescence would be higher than in the absence of gap vortices. One may thus infer that, for a fixed j_l in a strongly eccentric channel, the flow would cross the regime boundary at a j_g that is lower than that in a concentric channel. Alternatively, for a fixed j_g in a strongly eccentric channel, the flow would cross the regime boundary at a higher j_j than that in a concentric channel. A related but separate effect is that bubbles, which otherwise would tend to concentrate in the wider part of the channel where friction effects are less significant, would cross the narrow gap, where they are more likely to collide with other bubbles and coalesce. Although hydrodynamic stability analysis (Moradi & Tavoularis, 2019) has shown that gap instability may be triggered for eccentricities as small as 0.05, in practice, strong gap vortex streets in turbulent flows would likely occur for $e \gtrsim 0.5$ (Lamarche-Gagnon & Tavoularis, 2021). In view of these considerations, we may plausibly attribute the apparent shift of the regime boundaries to the action of gap vortex streets. This explanation seems to be well justified for the bubbly-to-cap-bubbly and cap-bubbly-to-slug-flow transitions. The effect of strong eccentricity on the slug-flow-to-churn-flow transition seems to be also a shift towards higher j_g (or lower j_l), although the available information is insufficient for us to describe the precise mechanism that causes this phenomenon.

CONCLUSIONS

For the first time in the literature, an upward gas-liquid flow regime map was created for an annular channel with the full range of eccentricity. The map extended over four flow regimes, namely, bubbly, cap-bubbly, slug and churn flow and had sufficient resolution to identify the regime transition regions. It was found that eccentricity in the range from 0.3 to 0.7 affected the transition from one regime to another. In particular, the transitions from bubbly to cap-bubbly flow and from cap-bubbly to slug flow under a constant water superficial velocity were shifted towards higher air superficial velocities. Flow visualisation showed the presence of oscillatory cross flows in the bubbly, cap-bubbly and slug flow regimes for $e = 0.5$ and 0.7. Such cross flows were also observed in numerical simulations. The presence of a gap vortex street was identified as the cause for cross flows and explained the effect of eccentricity on regime transition. The present study has complemented and expanded the literature on gas-liquid flows in annular channels and has shown that eccentricity has significant effects. It has further provided evidence for the presence of gap vortex streets in gas-liquid flows, thus connecting to the substantial literature for single-phase flows in channels with narrow gaps.

REFERENCES

Barnea, D. 1987 A unified model for predicting flow-pattern transitions for the whole range of pipe inclinations. *Int. J. Multiph. Flow* **13** (1), 1–12.

Bilgin, E.O. 2026 Gas-liquid Flows in Vertical Annular Channels. PhD thesis, University of Ottawa, ON, Canada.

Brennen, C.B. 2005 *Fundamentals of Multiphase Flow*. Cambridge University Press, Cambridge, UK.

Caetano, E.F., Shoham, O. & Brill, J.P. 1992*a* Upward vertical two-phase flow through an annulus—Part I: Single-phase friction factor, Taylor bubble rise velocity, and flow pattern prediction. *J. Energy Resour. Technol.* **114 (1)**, 1–13.

Caetano, E.F., Shoham, O. & Brill, J.P. 1992*b* Upward vertical two-phase flow through an annulus—Part II: Modeling bubble, slug, and annular flow. *J. Energy Resour. Technol.* **114 (1)**, 14–30.

Cao, F., Dang, R., Dang, B., Zheng, H., Ji, A., Chen, Z., Zhao, J. & Sun, Z. 2024 Flow regimes identification of air water counter current flow in vertical annulus using differential pressure signals and machine learning. *Scientific Reports* **14** (1), 12572.

Choueiri, G.H. & Tavoularis, S. 2014 Experimental investigation of flow development and gap vortex street in an eccentric annular channel. Part 1. Overview of the flow structure. *J. Fluid Mech.* **752**, 521–542.

Choueiri, G.H. & Tavoularis, S. 2015 Experimental investigation of flow development and gap vortex street in an eccentric annular channel. Part 2. Effects of inlet conditions, diameter ratio, eccentricity and reynolds number. *J. Fluid Mech.* **768**, 294–315.

Das, G., Das, P.K., Purohit, N.K. & Mitra, A.K. 1999 Flow pattern transition during gas liquid upflow through vertical concentric annuli—part I: Experimental investigations. *J. Fluids Eng.* **121** (4), 895–901.

De Sousa, P.C., Falcone, G. & Barrufet, M. 2014 Upward gas-liquid flow in concentric and eccentric annular spaces. In *SPE Latin America and Caribbean Petroleum Engineering Conference*, p. D021S015R005. Maracaibo, Venezuela, 21-23 May 2014, Society of Petroleum Engineers.

Guo, R., Chen, Y., Waltrich, P. J & Williams, W.C. 2018 An experimental investigation on flow pattern map and drift-flux model for co-current upward liquid-gas two-phase flow in narrow annuli. *J. Nat. Gas Sci. Eng.* **51**, 65–72.

Hetsroni, G. 1982 *Handbook of Multiphase Systems*. McGraw-Hill Book Co., New York, NY.

Hibiki, T. & Mishima, K. 2001 Flow regime transition criteria for upward two-phase flow in vertical narrow rectangular channels. *Nucl. Eng. Des.* **203** (2-3), 117–131.

Hibiki, T., Situ, R., Mi, Y. & Ishii, M. 2003 Local flow measurements of vertical upward bubbly flow in an annulus. *Int. J. Heat Mass Transf.* **46** (8), 1479–1496.

Julia, J.E. & Hibiki, T. 2011 Flow regime transition criteria for two-phase flow in a vertical annulus. *Int. J. Heat Fluid Flow* **32** (5), 993–1004.

Julia, J.E., Ozar, B., Dixit, A., Jeong, J.J., Hibiki, T. & Ishii, M. 2009 Axial development of flow regime in adiabatic upward two-phase flow in a vertical annulus. *J. Fluids Eng.* **131** (2).

Julia, J.E., Ozar, B., Jeong, J.J., Hibiki, T. & Ishii, M. 2011 Flow regime development analysis in adiabatic upward two-phase flow in a vertical annulus. *Int. J. Multiph. Flow* **32** (1), 164–175.

Kelessidis, V.C. & Dukler, A.E. 1989 Modeling flow pattern transitions for upward gas-liquid flow in vertical concentric and eccentric annuli. *Int. J. Multiph. Flow* **15** (2), 173–191.

Kelessidis, V.C. & Dukler, A.E. 1990 Motion of large gas bubbles through liquids in vertical concentric and eccentric annuli. *Int. J. Multiph. Flow* **16** (3), 375–390.

Kiran, R., Ahmed, R. & Salehi, S. 2020 Experiments and CFD modelling for two phase flow in a vertical annulus. *Chem. Eng. Res. Des.* **153**, 201–211.

Lamarche-Gagnon, M.-É. & Tavoularis, S. 2021 Further experiments and analysis on flow instability in eccentric annular channels. *J. Fluid Mech.* **915**, A34.

Liu, Y., Mitchell, T., Upchurch, E.R., Ozbayoglu, E.M. & Baldino, S. 2024 Investigation of Taylor bubble dynamics in annular conduits with counter-current flow. *Int. J. Multiph. Flow* **170**, 104626.

Mishima, K. & Ishii, M. 1984 Flow regime transition criteria for upward two-phase flow in vertical tubes. *Int. J. Heat Mass Transf.* **27** (5), 723–737.

Moradi, H.V. & Tavoularis, S. 2019 Flow instability in weakly eccentric annuli. *Phys. Fluids* **31**, 044104.

Oshinowo, T. & Charles, M.E. 1974 Vertical two-phase flow part I. Flow pattern correlations. *Can. J. Chem. Eng.* **52** (1), 25–35.

Ozar, B., Jeong, J.J., Dixit, A., Julia, J.E., Hibiki, T. & Ishii, M. 2008 Flow structure of gas–liquid two-phase flow in an annulus. *Chem. Eng. Sci.* **63** (15), 3998–4011.

Sadatomi, M., Sato, Y & Saruwatari, S. 1982 Two-phase flow in vertical noncircular channels. *Int. J. Multiph. Flow* **8** (6), 641–655.

Sun, X., Kuran, S. & Ishii, M. 2004 Cap bubbly-to-slug flow regime transition in a vertical annulus. *Exp. Fluids* **37** (3), 458–464.

Taitel, Y., Barnea, D. & Dukler, A.E. 1980 Modelling flow pattern transitions for steady upward gas-liquid flow in vertical tubes. *AIChE J.* **26** (3), 345–354.

Tavoularis, S. 2011 Rod bundle vortex networks, gap vortex streets, and gap instability: A nomenclature and some comments on available methodologies. *Nucl. Eng. Des.* **241** (7), 2624–2626.

Yin, B., Zhang, C., Ding, T., Chen, C., Feng, K., Wang, Z. & Sun, B. 2025 An experimental and numerical study of gas-liquid two-phase flow moving upward vertically in larger annulus. *Eng. Appl. Comput. Fluid Mech.* **19** (1), 2476605.